Energy 229 (2021) 120647

Contents lists available at ScienceDirect

Energy

journal homepage: www.elsevier.com/locate/energy

Ensemble of machine learning and spatiotemporal parameters to forecast very short-term solar irradiation to compute photovoltaic generators' output power

Fermín Rodríguez [a, b, *], Fernando Martín [a, b], Luis Fontán [a, b], Ainhoa Galarza [a, b]

[a] Ceit-Basque Research and Technology Alliance (BRTA), Manuel Lardizabal 15, 20018, Donostia/San Sebastián, Spain
[b] Universidad de Navarra, Tecnun, Manuel Lardizabal 13, 20018, Donostia/San Sebastián, Spain

ARTICLE INFO

Article history:
Received 20 October 2020
Received in revised form
23 January 2021
Accepted 10 April 2021
Available online 21 April 2021

Keywords:
Photovoltaic generation
Solar irradiation
Spatiotemporal forecaster
Artificial intelligence
Very short-term forecasting

ABSTRACT

Photovoltaic generation has arisen as a solution for the present energy challenge. However, power obtained through solar technologies has a strong correlation with certain meteorological variables such as solar irradiation, wind speed or ambient temperature. As a consequence, small changes in these variables can produce unexpected deviations in energy production. Although many research articles have been published in the last few years proposing different models for predicting these parameters, the vast majority of them do not consider spatiotemporal parameters. Hence, this paper presents a new solar irradiation forecaster which combines the advantages of machine learning and the optimisation of both spatial and temporal parameters in order to predict solar irradiation 10 min ahead. A validation step demonstrated that the deviation between the actual and forecasted solar irradiation was lower than 4% in 82.95% of the examined days. With regard to the error metrics, the root mean square error was 50.80 W/m^2, an improvement of 11.27% compared with the persistence model, which was used as a benchmark. The results indicate that the developed forecaster can be integrated into photovoltaic generators' to predict their output power, thus promoting their inclusion in the main power network.

1. Introduction

Currently, some countries' power systems are facing the same challenges with regard to increasing energy demand from customers and the limitations and negative consequences of fossil fuels [1,2]. In the present scenario, renewable resources, and solar photovoltaic (PV) generation in particular, have been proposed as a suitable solution. As the International Energy Agency states in its 2017 annual report [3], the total PV installed capacity exceeded 400 GW. Throughout 2017 the solar PV installed capacity grew by 99 GW, which means an increase of approximately 25% [4]. Given both documents [3,4], it is expected that the trend in PV penetration will continue to grow in the following years.

Traditionally, the most difficult challenge in power systems is the ability to balance both generation and demand at every moment. It is for this reason that unit-commitment and economic-dispatch strategies have been used to guarantee efficient use of the generation mix and a safe electricity supply [5]. In order to offer these guarantees, synchronous conventional technologies such as hydro [6], thermal [7] or nuclear power have been used by power system operators in order to fulfil their network requirements in brief time lapses. However, PV generation is not deterministic due to the fact that it is not possible to determine a following state from the previous ones, which makes this kind of energy generation difficult to control. Hence, the integration of future PV plants into the main grid is limited by the uncertainty and intermittence of meteorological parameters involved in this technology's production, such as solar irradiation or the clear sky index [8]. Therefore, the integration of more renewable generators will increase the traditional grid's uncertainty level due to these generators' dependency on intermittent meteorological parameters. In order to be able to continue adding renewable generators in traditional networks, main grid operators have started asking that the operating requirements for renewable resources be increased in order to make them as reliable as conventional generators in the medium-term. For instance, an option to improve the reliability of renewable generators consists of increasing the accuracy of

* Corresponding author. Ceit-Basque Research and Technology Alliance (BRTA), Manuel Lardizabal 15, 20018, Donostia/San Sebastián, Spain.
E-mail address: frlalanne@ceit.es (F. Rodríguez).

https://doi.org/10.1016/j.energy.2021.120647

prediction for the above mentioned parameters [9]. To that end, this study will focus on building a forecaster that is able to predict solar irradiation and is sufficiently accurate to compute PV solar output generation and support this technology integration in traditional networks.

Solar irradiation forecasters can be described in terms of two primary dimensions: the first relies on the forecaster's prediction horizon and the second is based on the model that is used to develop the forecaster. The prediction horizon dimension contains four types of forecasters [10]: a) very short-term forecasters, whose predictions are made for next few minutes and are involved in real-time dispatch [11,12]; b) short-term forecasters, whose predictions are made from a few hours ahead up to a day ahead and where the predicted values are involved in unit-commitment or economic-dispatch [13,14]; c) medium-term forecasters, whose predictions are made over a range from a day to a few weeks, and the predicted values are used in maintenance planning [15]; and d) long-term forecasters, whose predictions are made for a range from a few weeks to months ahead and where the predicted values are used to power assessment and examine the necessity of new power infrastructures [16,17].

The second dimension classifies solar irradiation forecasters into physical, statistical or artificial intelligence models. Physical models include all forecasters which are based on numerical weather prediction (NWP) [18,19] or sky imagery [1,20,21]; statistical models group forecasters which rely on historical databases and time series, such as autoregressive moving average [22] and seasonal autoregressive integrated moving average [23]; and artificial intelligence models include forecasters that have the capacity to establish nonlinear correlations among the system's input and output parameters, such as support vector machines (SVM) [24] and artificial neural networks (ANN) [25].

Designing forecasters which are based on NWP models is not easy, due to the fact that it is necessary to have in-depth knowledge about the physical equations and parameters that are involved in solar irradiation evolution [26,27]. Regarding sky imagery-based forecasters development, it is not always possible to have the required equipment available due to its high cost. These physical models are therefore usually rejected because of the complex knowledge involved or high cost of the equipment. Statistical models are useful for forecasting values when a physical system's input and output parameters are governed by linear relationships. However, solar irradiation's unexpected changes are not governed by linear relationships, and so statistical models must be combined with other ones [5,23], such as artificial intelligence-based approaches, in order to be able to predict sudden changes. As a consequence, in this research different artificial intelligence algorithms are analysed with the aim of selecting the most accurate one to develop our forecaster.

The first artificial intelligence models, also known in the last few years as machine learning models, were endogenous, which means that they just used historical time series data for the parameter that was to be predicted at the target site [28,29]. As there was great need to improve the accuracy of forecasters for the very short-term and short-term horizons in order to support the penetration of new PV plants, some authors suggested using other parameters, such as solar irradiation values from nearby sites [30] or other meteorological parameters like relative humidity or temperature [31,32]. Nevertheless, the main challenge that these models were not able to overcome was the huge amount of data that was managed and the associated high computational cost. Therefore, it was necessary to develop new algorithms. Once the algorithms were improved, researchers focused on using available spatial and temporal historical databases close to a target location for new models [33]. In the literature, forecasters which use spatial and temporal databases are called spatiotemporal approaches [34,35], where spatial databases take into account the available data from stations surrounding the target location and temporal databases examine the amount of past data that should be taken into account.

A literature review indicates that some authors suggested the combination of statistical models and spatiotemporal databases. For instance, Tascikaraoglu et al. [36] proposed a compressive spatiotemporal forecaster to predict not only meteorological parameters such as temperature, solar irradiation or wind speed, but also power output obtained through PV panels in a very short-term horizon, i.e. next 15 min. Although Tascikaraoglu's error metric results do not demonstrate a large improvement in forecasted value accuracy, if the spatiotemporal forecaster's results are analysed, it can be seen how forecasted values follow the trend of actual values with better accuracy. Concerning solar irradiation error metrics, Tascikaraoglu's model obtains a root mean squared error (RMSE) and a normalised root mean squared error (NRMSE) of 77.76 W/m^2 and 6.72%, respectively, for a whole year. In addition, Agoua et al. [37] developed a method based on combining equations whose coefficients were optimised by sliding intervals of simulated solar irradiation values. The information provided by a group of sensors divided among 185 PV plants were used as inputs to the model to improve the forecaster's accuracy in the very short-term (0–6h). Results provided by Agoua et al.'s model demonstrate a range of improvement from −0.46% to 20.13% in the RMSE for the analysed period of time. However, few authors have examined the combination of machine learning and spatiotemporal databases. For instance, Zhao et al. [38] proposed a forecaster where the combination of a 3D convolutional neuronal network and spatiotemporal database was analysed. Zhao et al.'s model analyses consecutive ground-based cloud images to obtain temporal information and previous direct normal irradiance values to predict direct normal irradiance in the very short-term (10–30min). In Ref. [38], Zhao et al. presented information about different error metrics for each analysed prediction horizon; for 10-, 20- and 30-min prediction horizons the NRMSE values were 30%, 34% and 39%. From the available literature [36–38], we concluded that applying spatiotemporal databases to previously developed forecasters improves their accuracy.

In recent years, new artificial intelligence approaches for developing very short-term solar irradiation forecasters, such as recurrent neural networks (RNN) [39] or long short-term memory networks (LSTMN), have been proposed [40,41]. In the present study, we examine the ensemble of some of these new artificial intelligence approaches using spatiotemporal databases in order to analyse the evolution in solar irradiation forecasting and after that, compute PV generator's output power. The key contributions of this research are as follows:

1) The main innovation of this research is the development of a very short-term solar irradiation forecaster, for a 10-min prediction horizon, to calculate solar output power. The forecaster relies on the ensemble of a feedforward neural network and a spatiotemporal approach.
2) After running several sensitivity analyses, we conclude that the following parameters are needed by the novel forecaster to make more accurate predictions: "season", "forecast time", "relative position among target and chosen locations", and "solar irradiation data from the target and chosen locations during the last 24 h".
3) Because there is a huge number of models in the literature, the most popular models were tested in order to select the most accurate one and use it to develop the proposed model. In addition, RMSE and other error metrics were calculated to analyse the deviation between actual and predicted values

within the tested methods in this research, and also against results provided by other authors.

This paper is organised as follows. In Section 2, the most popular solar irradiation forecasters are described, along with the proposed model. In Section 3, the results obtained by the optimised model are analysed, and they are compared against those presented by other authors through their forecasters for similar prediction horizons. This section also analyse the accuracy of solar PV generators' output power computation. The conclusions that can be drawn from this research are given in Section 4.

2. Methodology

As described in Section 1, in recent years different models for forecasting very short-term solar irradiation have been proposed. We intend to apply our forecaster to address the real-time control challenges that come up with the use of renewable generators, so our forecaster is classified in this prediction horizon. Although some authors propose combining the single approaches presented above to increase the accuracy of the forecasters, this option is usually applied to develop forecasters with short-term prediction horizon or longer [14,42], though it must be taken into account that the longer the prediction horizon, the lower the accuracy of the forecasters [13,25,30]. Forecasters which are based on the combination of two or more models are commonly called multiple or hybrid models. While some authors support multiple models for very short-term forecasters [1,23,43], other studies in the literature have presented similar error metric and accuracy results with single-approach forecasters [13,17,40]. After reviewing the available literature and comparing the results obtained by those studies, we chose a single model forecaster to develop our approach.

The methodology used to develop our forecaster will be presented as follows. Firstly, different single-model approaches will be analysed to select the model that performs best for solar irradiation forecasting at the target station; secondly, the data from the stations surrounding the target location will be examined to select only those that have relevant information and finally, different spatiotemporal input vectors are constructed and a sensitivity analysis is conducted to select the optimal number of stations for our approach.

2.1. Models studied

Several studies proposing solar irradiation forecasters based on machine learning algorithms appear in the literature. Some of the most widely cited are feed forward neural networks (FFNN) [31,35], recurrent neural networks (RNN) [39], wavelet neural networks (WNN) [25], support vector machines (SVM) [24,44], support vector regression (SVR) [45], fuzzy logic (FL) [46] or genetic algorithms (GA) [47]. While FFNNs, RNNs and WNNs are based on a replication of human brain's capacity to generate relationships in nonlinear systems, SVMs and SVRs rely on the generation of different equations for different states of a system. With regard to FL or GAs, these models try to generalise classical logic to predict the desired parameter. Of the above algorithms, we chose to examine FFNNs, RNNs and SVMs in developing our proposed forecaster because they are easy to implement and recent studies have demonstrated the accuracy of their predictions [24,29,33,37,44].

2.1.1. Persistence model

Very short-term forecasters based on persistence models are easy to program. Thus, these models are commonly used as benchmarks to make a comparison against new developed forecasters. This model is based on the assumption that no variation will occur in the value of a certain parameter between the present moment and the desired forecast moment.

$$P(t+h) = P(t) \tag{1}$$

where $P(t + h)$represents the prediction made for the chosen prediction horizon h and $P(t)$ is the present value of the predicted parameter.

Meteorological parameters are strongly correlated when the time lapse between two steps is small. Therefore, for very short-term and short-term prediction horizons, not only does the correlation become stronger, but the accuracy of the forecaster also increases. Nevertheless, this model just relies on a single previous value to forecast the desired parameter. As this model is not able to predict sudden changes, its accuracy is reduced when such changes occur.

2.1.2. Artificial neural network models

ANNs rely on the combination of computational algorithms and the replication of the human brain. These models are based on an architecture where a single unit is called a neuron, after the real biological structure [48]. The neurons of the system are linked by synaptic junctions, which have the ability to transfer the information not only from different inputs but also from other neurons. Each neuron sums all the information that it receives through the synaptic junctions, and if this value surpasses a threshold the neuron will send an output to the following neuron. The ability to produce accurate outputs from previously unseen values makes ANNs suitable for developing new very short-term and short-term forecasters [49].

In addition, ANNs have the advantage of being able to predict sudden changes, as they are modelled by nonlinear activation functions and trained through supervised learning algorithms. Of all possible ANNs, in this study FFNNs and RNNs are examined based on the accuracy error metric results from recent studies reported in the literature [29,33,37] and their relative ease of implementation.

2.1.2.1. Feedforward neural networks. FFNNs are probably the most examined and implemented ANN. In this configuration, a small number of parameters, such as the number of layers, the number of neurons in each layer and the training algorithm, have to be fixed. The key advantages of FFNNs are that they are easy to program and they train more quickly compared to other models, and they are robust in the face of missing data. Moreover, in a FFNN information flows from input to output layers with no feedback; if the above parameters are fixed properly for each system, a well performing local approximator can be obtained [49].

2.1.2.2. Recurrent neural networks. RNNs are characterised by the incorporation of feedback loops into the information flow. These loops commonly go from the output of hidden layer, back to the input of the previous layer. In addition to fixing the same parameters as mentioned for FFNNs, these networks need a time delay function (z^{-t}). The incorporation of loops improves the generalisation capacity of the forecaster, thereby improving the accuracy of the forecaster in complex systems. The main drawback of this approach is that the training time required is much higher than for FFNNs.

2.1.3. Support vector machine models

SVM models are commonly applied in nonparametric systems where regression or data classification is a possible choice. For instance, in this study, which seeks to develop a very short-term solar irradiation forecaster, a regression SVM model will be

analysed. In the training step, a set of data and a kernel function are chosen to fix the parameters of the model. In contrast to ANNs, which do not have the ability to vary the chosen parameters during training step, SVMs are allowed to make this modification.

The kernel functions that SVMs use optimise the initial equation proposed by the model based on the chosen database. Throughout the learning step, the kernel function tries to reduce the error between the actual and forecasted values. Moreover, as said above, if during the training step the kernel function detects that a modification to the previously set parameters improves the accuracy of the forecaster, it will change them.

When the proper kernel function and database are chosen, a successfully fixed SVM regression model able to produce accurate predictions is obtained. However, if a big database is used for the training step, the model cannot be properly fixed because there is the risk of getting stuck in a local minimum instead of continuing to look for the best solution. Thus, if not converging on a local minimum is desired, it is necessary to choose a suitable kernel function and a representative piece of the database [50].

2.2. Proposed model

The model developed through this study relies on the combination of the most accurate forecaster from the models described above and a spatiotemporal historical database which includes information from different locations next to the target location. Our approach to model development is as follows. Firstly, several tests were run not only to optimise the single-approach structures but also to examine which of the approaches produced the most accurate solar irradiation prediction. Secondly, we analysed which stations around the target's location had recorded historic data for solar irradiation. Thirdly, we constructed different spatiotemporal databases which contain the information from the N-closest stations as well as the distance and the relative position between the target's location and the other stations' locations. After that, these databases were applied to the most reliable single-approach to train the structures of the novel forecaster. Lastly, we ran the validation step to analyse which forecaster was the most accurate. Fig. 1

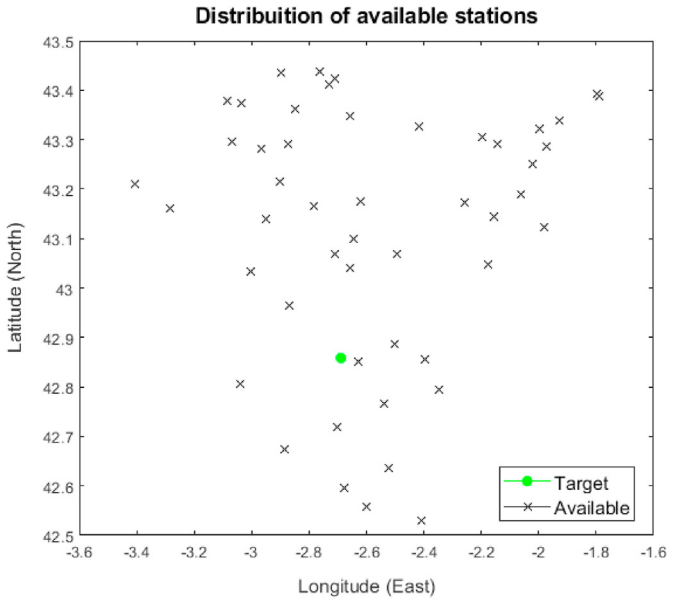

Fig. 1. Location of target (green dot) and available stations (black crosses). (For interpretation of the references to colour in this figure legend, the reader is referred to the Web version of this article.)

shows the result of the second step, where the coordinates are given to all the available meteorological stations in the Basque Country, Spain, each black cross representing the location of one meteorological station whose recorded data had been analysed to develop the most accurate forecaster. The green dot represents the target location, which is situated in Vitoria-Gasteiz, Spain.

2.3. Error metrics

Error metrics are commonly calculated in the current literature [1,13,14,17,40,43] to analyse and compare the accuracy improvement of new forecasters. Root mean square error (RMSE), mean absolute error (MAE) and mean absolute percentage error (MAPE) are usually the chosen error metrics. While the RMSE are to be used to compare the methods described in Section 2, other error metrics such as MAE and MAPE are also calculated to compare our results against the ones in the literature.

The RMSE, MAE and MAPE are defined as:

$$RMSE = \sqrt{\frac{1}{N}\sum_{i=1}^{N}(Y_i - Y_i')^2} \tag{2}$$

$$MAE = \frac{1}{N}\sum_{i=1}^{N}|Y_i - Y_i'| \tag{3}$$

$$MAPE = \frac{1}{N}\sum_{i=1}^{N}\left|\frac{(Y_i - Y_i')}{Y_i}\right| * 100\% \tag{4}$$

where Y_i is related to measured values; Y_i'refers to predicted values and N is the number of forecasts made in a range of time.

3. Numerical results and discussion

The historical meteorological databases used in this research were downloaded from the webpage belonging to Euskalmet, the Basque Government's Meteorological Agency. To examine which of the forecasters presented in Section 2 is more accurate, data from station 'C040', which is associated to Vitoria-Gasteiz, were chosen. The procedure was the same for each model; a historical database for the years 2015–2016 was applied for the training step and data from 2017 were used at the validation step. Because the data from 2017 were not previously used in the training step, the real accuracy of the forecaster can be examined. All the models explained in Section 2 were programmed in MATLAB®.

3.1. Results for the models presented in Section 2

3.1.1. Persistence model

Taking the deviation between the actual and forecasted values, RMSEs were calculated for the training and validation steps, yielding 59.47 W/m^2 and 57.25 W/m^2, respectively. Although it is not very common for the training RMSE to be bigger than the validation RMSE, this fact is related to the variability of the measurements recorded in the training database. Therefore, it is expected that this difference will persist throughout the research. Fig. 2 shows the evolution of actual and forecasted values for a specific sunny day, April 7, 2017. The actual solar irradiation measurements are represented by continuous blue line and the values forecasted by the model are given by the discontinuous orange one. The RMSE for this sample day was 20.09 W/m^2.

In addition, the values calculated for both databases were used as a reference to analyse the accuracy performance obtained

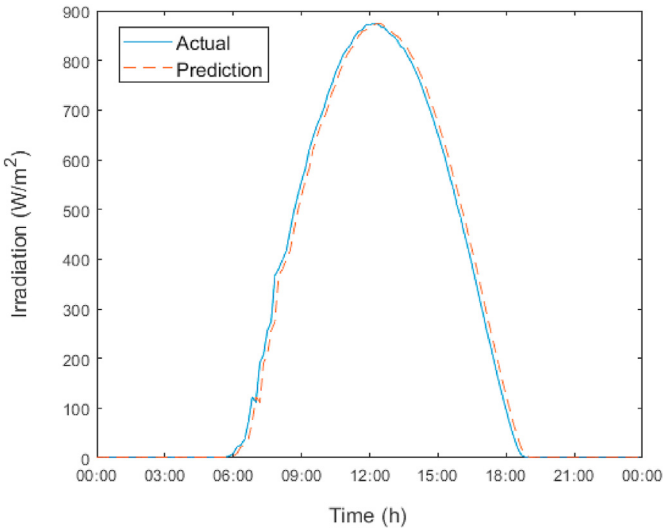

Fig. 2. Actual values vs. values forecasted by persistence model for April 7, 2017.

through other models. Equation (5) was used to examine this evolution:

$$\text{Performance } (\%) = \frac{RMSE_{reference} - RMSE_{model}}{RMSE_{reference}} * 100 \quad (5)$$

where $RMSE_{reference}$ will be always the RMSEs calculated by the persistence model for training or validation steps, and $RMSE_{model}$ will be related to the RMSE models that are being compared.

3.1.2. Feedforward neural network

With regard to learning algorithms, the vast majority of authors [25,39,51] report that Levenberg-Marquardt (LM) is the best option for developing FFNN forecasters. After reviewing related literature [10,23,39,40], it was evident that no methodology had been developed recently to fix the parameters involved, such as the number of neurons per layer. That meant that an iterative process needed to be chosen in order to fix them. The final structure of the FFNN is based on a 3-layer network; the first layer is used to introduce inputs, the second layer performs the internal calculations, and the third layer gives the forecast value.

In terms of the iterative process used to fix the number of neurons in the hidden layer, several configurations were examined, and the results are summarised in Table 1. When MATLAB® is used to train a forecaster, a random initialisation occurs; to reduce the possibility of getting to a local minima, five tests were run for each configuration. Table 1 presents each configuration's average RMSE value for those five training and validation tests. The input vector contains "season", "time of day" and "data with a 10-min sampling period from the previous 24 h of solar irradiation measurements".

Table 1
Average results for training and validation steps in fixing the FFNN parameters.

Configuration	Neurons	RMSE train. (W/m^2)	RMSE val. (W/m^2)
1	2	55.38	53.20
2	4	54.43	52.69
3	5	54.41	**52.65**
4	6	54.26	52.67
5	8	54.00	52.77
6	10	53.43	53.06
7	15	53.16	53.17
8	20	**52.55**	53.66

As can be seen in Table 1, while the most optimal training RMSE is obtained for 20 neurons structure, the lowest RMSE for the validation database is obtained for a 5-neuron architecture. Taking into account that a forecaster's capacity is based on its ability to produce accurate predictions with previously unseen values, the 5-neuron structure was chosen as the most reliable architecture. Fig. 3 presents the evolution of actual and predicted values for April 7, 2017 for this forecaster. The RMSE calculated for this sample day was 10.09 W/m^2; this is an accuracy improvement of 49.77% compared against the persistence model.

Finally, if the results obtained through the optimised FFNN are compared against the results from the persistence model, they improve from 59.47 W/m^2 to 54.41 W/m^2 in the training step and from 57.25 W/m^2 to 52.65 W/m^2 in the validation step. This represents an accuracy improvement of 8.51% and 8.03% in the learning and validation steps, respectively.

3.1.3. Recurrent neural network

In this model, it is necessary to fix not only the number of neurons in the hidden layer but also the delay associated with the feedback loops. For this purpose, the number of neurons was maintained constant while the delay was modified from 2 to 6 time steps. Once the delay giving the lowest error was detected, it was kept constant while the number of neurons was varied from 5 to 20. Like in the FFNN's training step, MATLAB® introduces a random initialisation whose effect has been minimised by repeating each configuration five times. Table 2 presents the average RMSE values for those five training and validation tests. As for the input vector for the RNN training, it had the same parameters as the FFNN model.

From these tests, it was concluded that the configuration delay of 1:2 and 10 neurons in the hidden layer minimises the RMSE for both training and validation steps. Fig. 4 shows the trend for the actual and predicted values for April 7, 2017 through the RNN forecaster. The RMSE calculated for this sample day was 10.49 W/m^2.

If these results are compared against the benchmark, there is improvement not only in the training step (where values went from 59.47 W/m^2 to 54.43 W/m^2), but also in the validation step (where values went from 57.25 W/m^2 to 52.85 W/m^2). If these values are applied to Eq. (5), it entails an improvement of 8.47% and 7.69% in

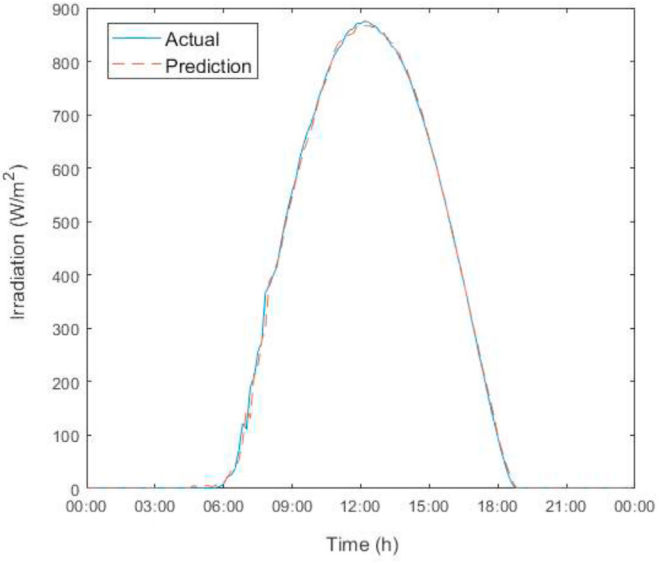

Fig. 3. Actual values vs. the FFNN model's predictions for April 7, 2017.

Table 2
Average results for training and validation steps in fixing the RNN parameters.

Configuration	Delay	Neurons	RMSE train. (W/m^2)	RMSE val. (W/m^2)
1	**1:2**	**10**	54.43	**52.85**
2	1:3	10	55.02	53.78
3	1:4	10	54.48	53.22
4	1:5	10	54.53	53.28
5	1:6	10	55.11	52.87
6	1:2	5	53.85	52.89
7	1:2	15	55.76	53.45
8	1:2	20	**53.65**	53.11

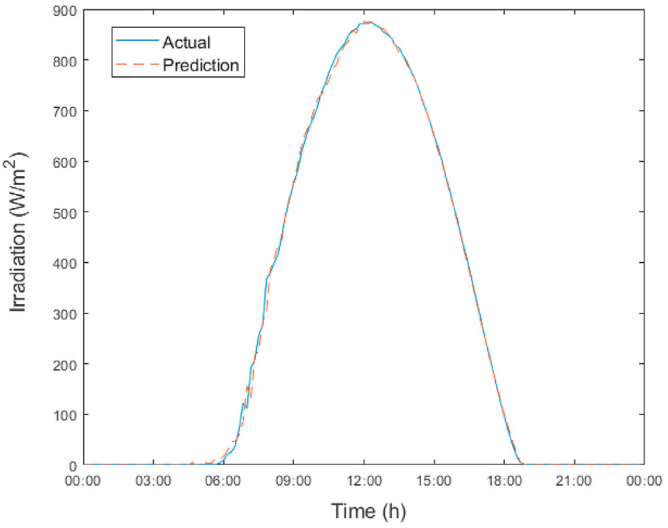

Fig. 4. Actual values vs. the RNN model's predictions for April 7, 2017.

the learning and validation steps, respectively. However, when compared with the FFNN structure, for solar irradiation forecasting the FFNN model slightly outperforms RNN model not only in the training step, where the difference is 0.02 W/m^2, but also in the validation step, where the improvement is 0.2 W/m^2.

3.1.4. Support vector machines

As illustrated in Table 3, different combinations of SVMs were implemented in this study. When designing SVMs, certain parameters, known as kernel functions and solvers, have to be chosen. As in the previous models, MATLAB® was used for the training, so in order to minimise the random initialisation five tests were run for each configuration. Table 3 presents the average RMSE for the training and validation steps.

The results in Table 3 suggest that the minimum RMSE is not obtained by the same configuration for both training and validation. While the 'SMO' solver and 'Radial Basis' function obtain the lowest RMSE in the training step, the 'ISDA' solver and 'linear' function obtain the lowest RMSE in the validation step. Because the objective of this study was to maximise the accuracy of the forecaster for previously unseen values, 'ISDA' solver and 'linear' function r was selected.

If the results of the selected configuration are compared against the persistence model, they improve in training step (from 59.47 W/m^2 to 56.47 W/m^2) and in validation step (from 57.25 W/m^2 to 54.19 W/m^2). If these figures are introduced in Eq. (5), this supposes an accuracy improvement of 5.04% and 5.34% in the learning and validation steps, respectively. Fig. 5 shows the actual and predicted values curves for April 7, 2017 from the SVM forecaster. The RMSE calculated for this sample day was 14.28 W/m^2, which means an accuracy improvement of 28.91%.

3.2. Proposed model: FFNN & SpatioTemporal model (FFNNST)

An examination of the accuracy of the forecasters in Section 3.1 showed that the FFNN model surpasses the others for the application under study. Therefore, our forecaster is based on a combination of both the FFNN and spatiotemporal models. A first approach was made by analysing the evolution of the proposed forecaster's accuracy when the 5, 10 and 15 nearest stations to the target location were checked. Only those stations that recorded solar irradiation parameter in their database were taken into account.

With regard to the input vectors, they were constructed in a manner similar to the models proposed above. While in the previous models the input vector was formed by "season", "forecast time" and "previous 24 h solar irradiation data in 10 min sampling",

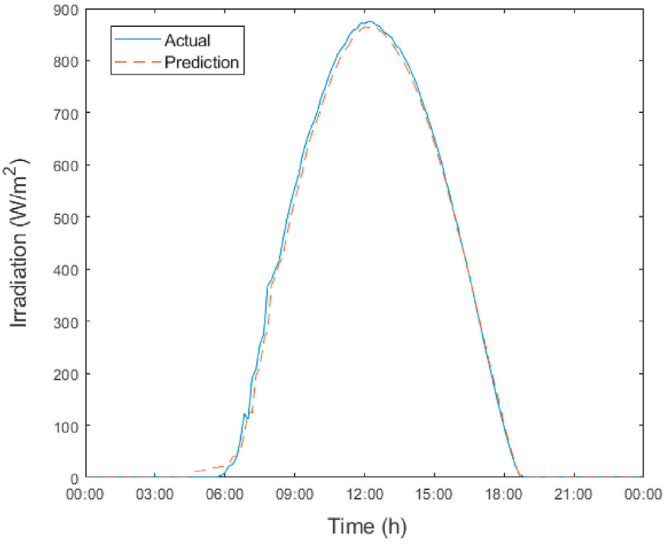

Fig. 5. Actual vs. the SVM model's predictions for April 7, 2017.

Table 3
Average results for training and validation steps in fixing the SVM parameters.

Solver	Kernel function	RMSE train. (W/m^2)	RMSE val. (W/m^2)
Sequential Minimal Optimisation (SMO)	Linear	56.52	54.24
	Gaussian	45.38	58.23
	Radial Basis	**45.27**	58.48
	Polynomial	54.05	68.33
Iterative Single Data Algorithm (ISDA)	Linear	56.47	**54.19**
	Gaussian	50.01	57.86
	Radial Basis	50.09	58.61
	Polynomial	63.38	71.34

this new forecaster adds not only the solar irradiation data for the selected nearest stations but also the relative position (distance and orientation) between each station and the target station.

As was done with single-model forecaster, the training historical database was formed by solar irradiation measurements from years 2015 and 2016 and the validation was performed with data from 2017. To develop this novel forecaster, as happened for single models, a solution was not found for the random initialisation issue or for selecting the optimal number nearest locations. While the feedforward neural network spatiotemporal (FFNNST) forecaster's architecture contains the 5 neurons from the FFNN's architecture, the number of stations around the target location has to be chosen. Thus, a sensitivity analysis was used to fit the number of nearest stations, the results of which are shown in Table 4.

Like in the analysis of single models, the maximum accuracy (lower RMSE) is not achieved by the same configuration for both training and validation datasets. While the configuration that considers the 15 closest locations to the target location gets the lowest training RMSE, the one that takes into account the 5 closest locations obtains the most accurate predictions when the validation dataset is used. In addition, there is also a trend discrepancy between both training and validation databases; while there is a direct relationship in the training dataset, namely the higher number of locations, the lower the RMSE, there is an absolute minima in the validation database for the 5 nearest locations configuration, 51.08 W/m^2.

Because the accuracy of a forecaster is based on its capacity to make accurate predictions by using previously unseen values, a deeper analysis was carried out in order to examine the evolution of accuracy between 1 and 10 nearest locations (see Table 5).

Based on the results provided by the tests presented in Table 5, the FFNNST forecaster was formed by the 7 nearest stations to the target location. Fig. 6 and Table 6 present the locations in both absolute and relative terms. In Fig. 6, the green dot marks the target's station's coordinates, the red triangles mark the position of the selected stations, and the black crosses indicate the coordinates of the available stations. However, as it is difficult to establish a relationship between each station and its coordinates in Fig. 6, Table 6 lists all the information associated to the selected stations. Fig. 6 shows that some stations close to the target location were not chosen for the final forecaster; these stations were not selected for different reasons, such as they do not record solar irradiation or there is a large amount of missing data in their databases.

When the results of the chosen configuration for the FFNNST forecaster are compared against the benchmark, accuracy in the training step improves from 59.47 W/m^2 to 52.76 W/m^2, and in the validation step it goes from 57.25 W/m^2 to 50.80 W/m^2. If these values are translated to a percentage by Eq. (5), this supposes an accuracy improvement of 11.28% and 11.27% in the learning and validation steps, respectively. This demonstrates that the proposed FFNNST model outperforms the other models analysed in this study. Fig. 7 shows the actual values and the FFNNST forecasters predicted value for April 7, 2017. The RMSE calculated for this sample day was 14.50 W/m^2, which means an accuracy improvement of 27.82%. Although it is true that for this sample day the RMSE is worse than in the single models, if the entire ranges of training and validation RMSE values are compared, the FFNNST model outperforms the single ones.

Table 4
Average results for fixing the FFNNST's parameters.

Configuration	Locations	RMSE train. (W/m^2)	RMSE val. (W/m^2)
1	1	54.41	52.65
2	5	51.53	**51.08**
3	10	50.38	51.61
4	15	**49.83**	52.37

Table 5
Average results to define the FFNNST parameter fixing.

Configuration	Locations	RMSE train. (W/m^2)	RMSE val. (W/m^2)
1	1	54.41	52.65
2	3	53.05	51.00
3	5	51.53	51.08
4	6	52.11	51.14
5	7	52.76	**50.80**
6	8	52.75	51.45
7	10	50.38	51.61

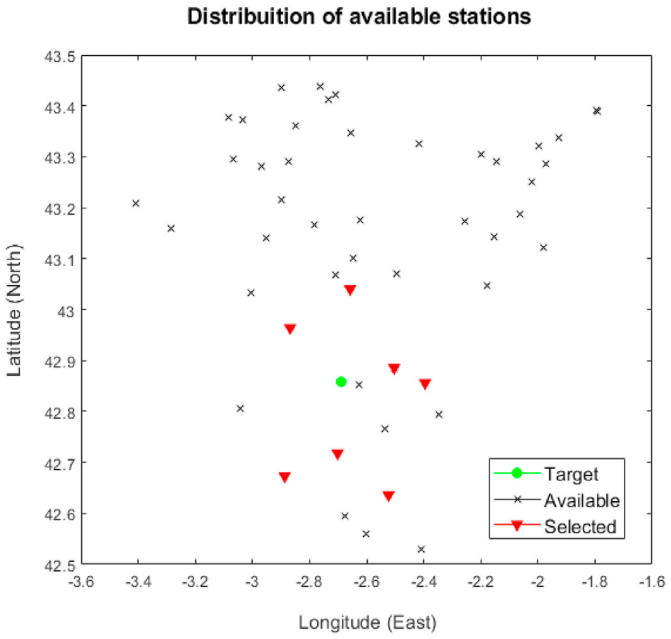

Fig. 6. Locations of target, selected and available meteorological stations.

In order to compare the accuracy of the FFNN and FFNNST models in different weather conditions, some sunny days, partially cloudy days and cloudy days were selected. Table 7 lists the calculated RMSE for each of the models studied and for the different types of days. It can be concluded from the results that in the vast majority of situations, the FFNNST forecaster outperforms the others, and in the cases where this does not happen, the results are close to the optimal result obtained by the FFNN.

Figs. 8 and 9 show how the values predicted by the forecaster follow the trend of actual measurements on partially cloudy and cloudy days.

In order to compare the results obtained by our proposed FFNNST forecaster against the results in the literature, two additional calculations were performed. Table 8 presents the calculations made through the error metrics defined in Section 2.3, and Fig. 10 presents a pie chart diagram that analyses the distribution of error made for days from 2017. This figure demonstrates that for 82.95% of the analysed days, the deviation between actual and predicted values is lower than 4%.

Having fixed the FFNNST forecaster's architecture and calculating some sample days, the next step was to examine the available literature [20,21,42,52] and compare published results against those calculated by the proposed FFNNST model. Although it is true that the comparison between the results provided by the proposed FFNNST forecaster and the results from the literature will be made

Table 6
Specific information about target and chosen locations.

Station	'Code'	Relative distance (km)	Longitude (°)	Latitude (°)
Target	'C040'	-	42.85	−2.68
Stations chosen for the FFNNST forecaster	'C035'	18.36	42.96	−2.88
	'C020'	15.63	42.72	−2.70
	'C041'	27.95	42.64	−2.52
	'C030'	23.15	42.85	−2.39
	'C054'	20.36	43.04	−2.66
	'C050'	25.84	42.67	−2.87
	'C0AA'	14.93	42.88	−2.50

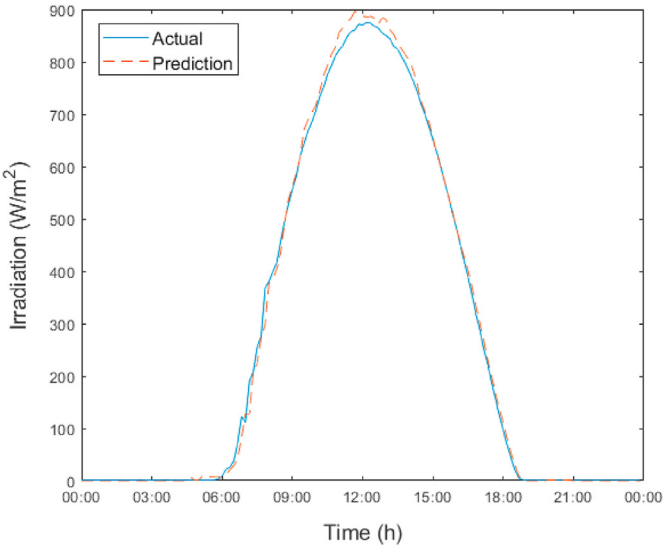

Fig. 7. Actual values vs. the FFNNST model's predictions for April 7, 2017.

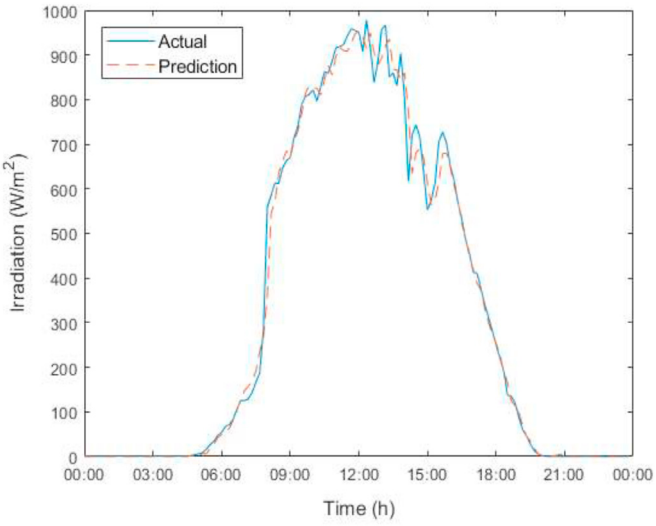

Fig. 8. Actual values vs. the FFNNST model's predictions for a partially cloudy day, June 10, 2017.

in terms of RMSE for a whole year or by sunny, partially cloudy or cloudy days, it must be noted that different databases were used. For instance, Elsinga et al. [20] proposed a "peer-to-peer" model that relies on the cross correlation between the clear-sky index and cloud movement sequence. If the results proposed in Ref. [20] are analysed, it can be concluded that while the peer-to-peer forecaster has high accuracy for clear or overcast days, its accuracy diminishes when partially or broken cloudy days are forecasted. Even though there are some results in Ref. [20] which demonstrate that Elsinga's model is better than our model for certain conditions, if the averaged values are contrasted, ours has a lower RMSE average value. While Elsinga et al.'s model has an average RMSE of 122 W/m^2 for low variability situations at a 9- to 12-min prediction horizon, the forecaster developed through this research has an average RMSE of 50.80 W/m^2 at a 10-min prediction horizon, which is an improvement of 58.36%.

Caldas et al. [21] suggested sky imagery be combined with real-time irradiance measurements to predict one to 10 min in advance. This model uses locally fixed pre-existing image processing models to estimate cloud movement, and thus their impact in solar irradiation, which makes it not only more expensive but also harder to implement. If 10 min in advance results for partially cloudy days are analysed, the calculated averaged RMSE and MAE are 251 W/m^2 and 168 W/m^2 [21], respectively. If Table 8 is examined for partially cloudy days, the FFNNST's RMSEs are range from 19.50 W/m^2 to 39.92 W/m^2, while the MAEs range from 7.55 W/m^2 to 19.23 W/m^2 so, the proposed model outperforms Caldas's one. Although Caldas's model outperforms this model in clear sky conditions (4.4 W/

Table 7
RMSE calculated for different situations by each proposed model.

Type of Day	Date	FFNN RMSE (W/m^2)	RNN RMSE (W/m^2)	SVM RMSE (W/m^2)	FFNNST RMSE (W/m^2)
Sunny	January 08, 2017	10.13	9.62	12.48	**9.58**
	April 12, 2017	17.13	17.18	17.82	**16.93**
	June 17, 2017	**6.08**	9.67	11.53	11.55
	November 20, 2017	10.57	10.07	11.89	**10.03**
Partially cloudy	January 04, 2017	**19.42**	19.56	21.03	19.50
	February 09, 2017	43.20	43.73	44.01	**39.92**
	April 03, 2017	33.26	33.46	34.97	**30.50**
	June 10, 2017	36.87	36.65	38.81	**31.88**
Cloudy	April 06, 2017	71.58	71.16	69.07	**67.14**
	June 02, 2017	83.66	84.40	81.83	**74.16**
	August 18, 2017	83.36	85.59	84.96	**72.69**
	September 02, 2017	71.09	70.74	72.14	**70.01**

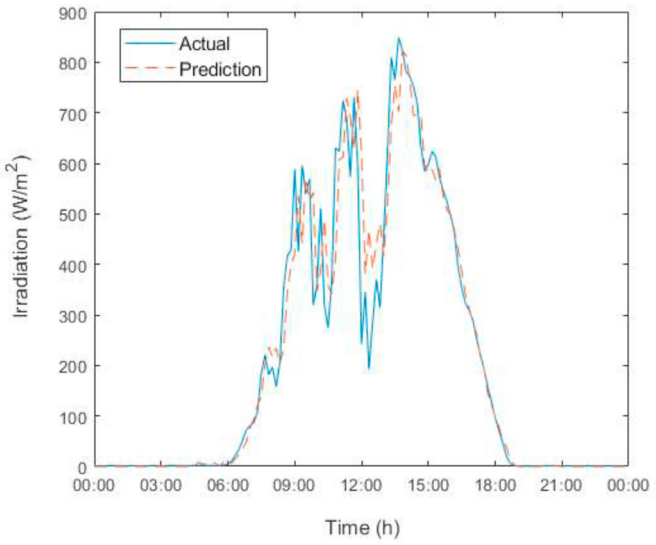

Fig. 9. Actual values vs. the FFNNST model's predictions for a cloudy day, April 6, 2017.

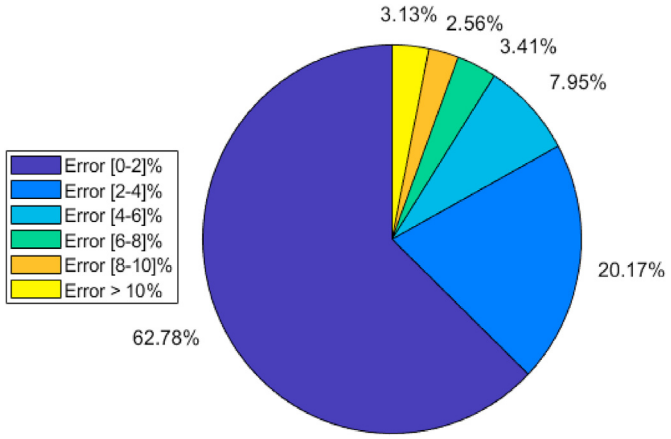

Fig. 10. Pie chart distribution of solar irradiation prediction error analysis for 2017.

m^2 vs. 9.58 W/m^2), our model outperforms Caldas's in overcast sky conditions (110 W/m^2 vs. 74.16 W/m^2). The forecaster's accuracy decreases on sunny days due to the fact that some minor variations in surrounding stations' solar irradiation measurements decreases the accuracy of FFNNST forecaster. Therefore, in follow up studies, the combination of FFNN for sunny days and FFNNST for the rest of the days will be examined.

Chu et al. [52] proposed a k-nearest neighbour ensemble forecast to model a probability density function to predict intra-hour solar irradiance (5, 10, 15 and 20 min ahead). Chu et al. demonstrated in Ref. [52] that their model outperformed the programmed persistence algorithm in all the locations studied. However, the provided error metrics are not divided among sunny, partially cloudy or cloudy day, which makes it difficult to compare the results from Chu et al. against those calculated in this study. Therefore, while the lowest RMSE for the 10-min prediction horizon provided by Chu et al. in Ref. [52] was 94.6 W/m^2 in the location of Merced, California, the highest error metric obtained through FFNNST's model is 74.16 W/m^2, which means an accuracy improvement of at least 21.24%.

PV generator's output power has been computed after concluding that developed solar irradiation FFNNST model's accuracy slightly improves literature studies' results. Equation proposed by Rodríguez et al. [39] and Yang et al. [53] has been applied to compute solar PV output power through meteorological parameters,

$$P_{PV}(t) = \eta * S * W(t) * (1 - 0.005 * (T(t) - 25)) \quad (6)$$

where, t refers to the selected prediction horizon (10 min in this study), $P_{PV}(t)$ is the PV generator's computed solar output power (W) for time t, η refers to generator's conversion efficiency, S is the PV generator's area (m^2), $W(t)$refers to forecasted solar irradiation value (W/m^2) for time t and T(t) is the ambient temperature ($^\circ C$) for time. Although temperature changes as solar irradiations do, Eq. (5) demonstrates that temperatures effect is lower than solar irradiation's. Therefore, in this study, it is assume that temperature is ruled by the persistence model where $T(t) = T(t + 10\text{min})$. To compute produced solar power a commercial panel was chosen whose technical characteristics are $\eta = 17.59\%$ and $S = 1.6767\ m^2$. Fig. 11a and b shows the trend of accumulated actual and predicted power values in both sunny and cloudy sample days. Fig. 11a shows the evolution in a sunny day January 8, 2017; whereas Fig. 11b presents the trend in a cloudy day August 18, 2017.

Concerning Fig. 11a where the deviation between actual and predicted accumulated energy trend is analysed in a sunny day, the difference among them is of 19.72 Wh which means a deviation of 2.51%. In Fig. 11b, the result of same analysis for a cloudy day is presented, in this case the difference between actual and forecasted accumulated energy is of 46.5 Wh, which means a deviation of 4.42%. In addition, both pictures (Fig. 11a and b) show how the trend in a sunny day is smoother than in a cloudy day where the trend has several bumps. Finally, Fig. 12 shows through a pie chart diagram the percentage deviation between actual and predicted accumulated energy for sample days into the period January to August 2017. The time period has been chosen to make it possible

Table 8
FFNNST forecaster's error metrics.

Type of Day	Date	RMSE (W/m^2)	MAPE (%)	MAE (W/m^2)
Sunny	January 08, 2017	9.58	5.25	5.15
	April 12, 2017	16.93	7.02	7.58
	June 17, 2017	11.55	5.27	7.45
	November 20, 2017	10.03	4.72	5.03
Partially cloudy	January 04, 2017	19.50	5.48	7.55
	February 09, 2017	39.92	8.75	19.23
	April 03, 2017	30.50	5.84	12.35
	June 10, 2017	31.88	6.19	16.13
Cloudy	April 06, 2017	67.14	17.28	31.47
	June 02, 2017	74.16	21.47	35.02
	August 18, 2017	72.69	20.32	34.22
	September 02, 2017	70.01	8.49	31.28

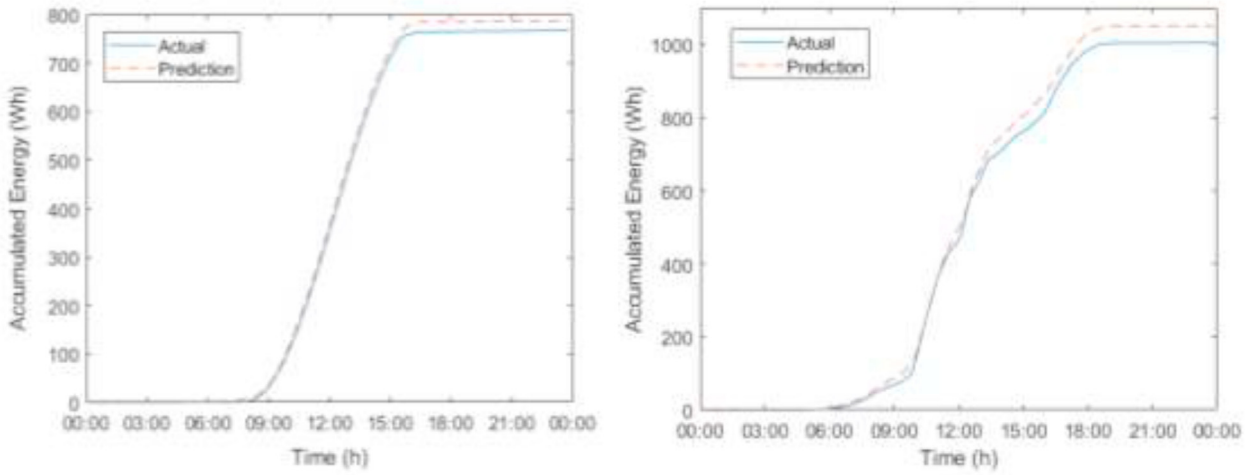

Fig. 11. a) Energy forecast for a sunny sample day, January 8, 2017 (left) and b) Energy forecast for a cloudy sample day, August 18, 2017 (right).

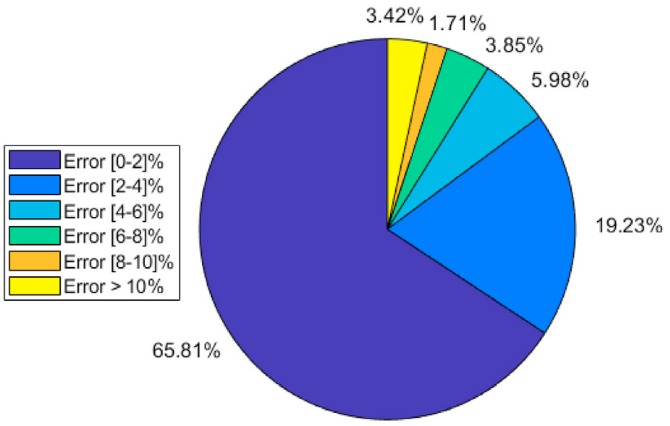

Fig. 12. Percentage distribution error for period January to August 2017.

the comparison of this study's results with the results obtained in a previous study [39].

While the FFNNST forecaster developed in this study achieved a deviation error rate under 2% for the 65.81% of the examined sample days, the RNN forecaster developed in Ref. [39] only got 56% of the days for same deviation error rate and period, January to August 2017. In addition, the average deviation error obtained in this study for the chosen period is 2.40%, whereas in the previous study it was 2.81%. Therefore, it is concluded that FFNNST forecaster provides more accurate and reliable solar irradiation values than RNN forecaster developed in previous study [39].

4. Conclusions

The purpose of this research was to develop a tool which is able to forecast solar irradiation 10 min ahead to compute PV generators' output power. Given the results obtained, this approach can be introduced in photovoltaic generator control to reduce their energy production uncertainty, making them more reliable for traditional network operators and therefore easier to integrate into traditional networks. The main conclusions of this research are as follows:

- Four different single approaches (persistence, FFNN, RNN and SVM) were programmed to forecast solar irradiation, and it was demonstrated that for this application the FFNN model was the most accurate in designing a single station forecaster. This model provided training and validation RMSEs of 54.41 W/m^2 and 52.65 W/m^2, respectively. These represent an accuracy improvement of 8.51% and 8.03% in the learning and validation steps, when compared against the benchmark persistence model.
- The FFNN structure was then combined with spatiotemporal optimisation to create the FFNNST forecaster. It was demonstrated that 7 locations maximise the accuracy of the forecaster. While the calculated RMSE for the learning and validation steps are 52.76 W/m^2 and 50.80 W/m^2, the associated error metrics in percentage are 11.28% and 11.27% respectively. In addition, this study demonstrates that FFNNST forecaster predictions are more accurate and reliable than the previous study's RNN forecaster, achieving a deviation error rate under 2% for the 65.81% of sample days.
- Comparative analyses of the RMSE error metric values for an entire year demonstrated that for cloudy and partially cloudy days the FFNNST forecaster outperforms the FFNN single-approach forecaster, while for sunny days there is either little improvement or the FFNN gives better results than the FFNNST does. This happens because small changes in solar irradiation at the surrounding stations will have a considerable impact on the target location. Therefore, in future studies we will analyse how to combine both forecasters (FFNNST and FFNN) in a single tool, where the prediction for sunny days will be done through the FFNN and the FFNNST will make predictions for the other days.
- All the calculations and results provided are based on real solar irradiation data from Vitoria-Gasteiz. For the training step, data from the years 2015–2016 were used, and for validation step data were from 2017. Although it has been demonstrated here that the FFNNST model definitively outperforms single models, it must be kept in mind that it will be necessary to fix not only the number of neurons of the FFNN but also the number of locations in the FFNNST model when it is implemented in any location.

Credit author statement

Fermín Rodríguez: Conceptualization, Methodology, Validation, Resources, Investigation, Writing – original draft. Fernando Martín: Methodology, Software, Investigation. Luis Fontán: Formal analysis, Supervision, Resources, Writing- Reviewing and Editing. Ainhoa

Galarza: Conceptualization, Visualization, Writing- Reviewing and Editing

Declaration of competing interest

The authors declare that they have no known competing financial interests or personal relationships that could have appeared to influence the work reported in this paper.

Acknowledgements

The authors would like to thank the Basque Government's Department of Education for financial support through the Researcher Formation Programme; grant number PRE_2019_2_0035.

References

[1] Takilalte A, Harrouni S, Rèdha Yaiche M, Mora-López L. New approach to estimate 5-min global solar irradiation dataon tilted planes from horizontal measurement. In: Renewable energy, vol. 145; 2020. p. 2477–88.
[2] Aguilar S, Telles GR, Medina P, Quaresma B, Cyrino FL, Castro R. Wind power generation: a review and a research agenda. J Clean Prod 2019;218:850–70.
[3] IEA, Trends. In photovoltaic applications. IEA-PVPS; 2018. http://www.iea-pvps.org/fileadmin/dam/intranet/task1/IEA_PVPS_Trends_2018_in_Photovoltaic_Applications.pdf. [Accessed 19 November 2019].
[4] Ren21, advancing the global renewable energy transition. https://www.ren21.net/wp-content/uploads/2019/08/Highlights-2018.pdf. (Accessed 25 November 2019).
[5] Fouilloy A, Voyant C, Notton G, Motte F, Paoli C, Nivet ML, Guillot E, Duchaud JL. Solar irradiation prediction with machine learning: forecasting models selection method depending on weather variability. In: Energy, vol. 165; 2018. p. 620–9.
[6] Liu Y, Qin H, Mo L, Wang Y, Chen D, Pang S, Yin X. Hierarchical flood operation rules optimization using multi-objective cultured evolutionary algorithm based on decomposition. In: Water resource management, vol. 33; 2019. p. 337–54.
[7] Qin H, Zhou J, Lu Y, Wang Y, Zhang Y. Multi-objective differential evolution with adaptive Cauchy mutation for short-term multi-objective optimal hydro-thermal scheduling. In: Energy conversion & management, vol. 51; 2010. p. 788–94.
[8] Voyant C, Guillot E. Solar irradiation nowcasting by stochastic persistence: a new parsimonious, simple and efficient forecasting tool. Renew Sustain Energy Rev 2018;92:343–52.
[9] Wang W, Li C, Liao X, Qin H. Study on unit commitment problem considering pumped storage and renewable energy via a novel binary artificial sheep algorithm. Appl Energy 2017;187:612–26.
[10] Majumder I, Behera MK, Nayak N. Solar power forecasting using a hybrid EMD-ELM method. In: International conference on circuits power and computing technologies. Kollam, India: ICCPCT; 2017.
[11] Singh SN, Mohapatra A. Repeated wavelet transform based ARIMA model for very short-term wind speed forecasting. In: Renewable energy, vol. 136; 2019. p. 758–68.
[12] Bouzgou H, Gueymard CA. Fast short-term global solar irradiance forecasting with wrapper mutual information. In: Renewable energy, vol. 133; 2019. p. 1055–65.
[13] Mathieu D, Mazorra L, Philippe L. Comparison of intraday probabilistic forecasting of solar irradiance using only endogenous data. In: International journal of forecasting, vol. 34; 2018. p. 529–47.
[14] Lopes FM, Silva HG, Salgado R, Cavaco A, Canhoto P, Collares-Pereira M. Short-term forecast of GHI and DNI for solar energy systems operation: assessment of the ECMWF integrated forecasting system in southern Portugal. In: Solar energy,, vol. 170; 2018. p. 14–30.
[15] Alonso J, Batlles FJ. Short and medium-term cloudiness forecasting using remote sensing techniques and sky camera imagery. In: Energy, vol. 73; 2014. p. 890–7.
[16] Carvallo JP, Larsen PH, Sanstad AH, Goldman C. Long term load forecasting accuracy in electric utility integrated resource planning. In: Energy policy, vol. 119; 2018. p. 410–22.
[17] Sharma A, Kakkar A. Forecasting daily global solar irradiance generation using machine learning. In: Renewable and sustainable energy reviews, vol. 82; 2018. p. 2254–69.
[18] Paulescu M, Paulescu E, Gravila P, Badescu V. Weather modeling and forecasting of PV systems operation. In: Springer. Solar radiation measurements. Springer-Verlag London; 2013. p. 17–42.
[19] Dong L, Wang L, Khahro SF, Gao S, Liao X. Wind power day-ahead prediction with cluster analysis of NWP. In: Renewable and sustainable energy reviews, vol. 60; 2016. p. 1206–12.
[20] Elsinga B, Gjhm van Sarck W. Short-term peer-to-peer solar forecasting in a network of photovoltaic systems. In: Applied energy, vol. 206; 2017. p. 1464–83.
[21] Caldas M, Alonso-Suárez R. Very short-term solar irradiance forecast using all-sky imaging and real time measurements. In: Renewable energy, vol. 143; 2019. p. 1643–58.
[22] Huang J, Korolkiewicz M, Agrawal M, Boland J. Forecasting solar radiation on an hourly time scale using Coupled AutoRegressive and Dynamical System (CARDS) model. Sol Energy 2013;83:342–9.
[23] Kushwaha V, Pindoriya NM. A SARIMA-RVFL hybrid model assisted by wavelet decomposition for very-short term solar PV power generation forecast". Renew Energy 2019;140:124–39.
[24] Jiang H, Dong Y. A nonlinear support vector machine model with hard plenty function based on glow worm swarm optimization for forecasting daily global solar irradiation. In: Energy conversion and management, vol. 126; 2016. p. 991–1002.
[25] Sharma V, Yang D, Walsh W, Reindl T. Short term solar irradiance forecasting using a mixed wavelet neural network. In: Renewable energy, vol. 90; 2016. p. 481–92.
[26] Reikard G, Haupt SE, Jensen T. Forecasting ground-level irradiance over short horizons: time series, meteorological, and time-varying parameter models. In: Renewable energy, vol. 112; 2017. p. 474–85.
[27] Tuohy A, Zack J, Haupt SE, Sharp J, Ahlstrom M, Dise S, Grimit E, Möhlren C, Lange M, Casado MG, Black J, Marquis M, Collier C. Solar forecasting: methods, challenges and performance. In: IEEE power energy management, vol. 13; 2015. p. 50–9.
[28] Cao J, Lin X. Study of hourly and daily solar irradiation forecast using diagonal recurrent wavelet neural networks. In: Energy conversion and management, vol. 49; 2008. p. 1396–406.
[29] Mellit A, Pavan AM. A 24-h forecast of solar irradiance using artificial neural network: application for performance prediction of a grid-connected PV plant at Trieste, Italy". In: Solar energy, vol. 84; 2010. p. 807–21.
[30] Lorenzo AT, Holmgren WF, Leuthold M, Kim CK, Cronin AD, Betterton EA. Short-term PV power forecasts based on a real-time irradiance monitoring network. In: IEEE 40th photovoltaic specialist conference. Denver, USA: PVSC); 2014.
[31] Sahoo AK, Sahoo SK. Energy forecasting for grid connected MW range solar PV system. In: 7th India international conference on power electronics. Patiala, India: IICPE); 2016.
[32] Tascikaraoglu A, Uzunoglu M. A review of combined approaches for prediction of short-term wind speed and power. In: Renewable and sustainable energy reviews, vol. 34; 2014. p. 243–54.
[33] Bessa RJ, Trindade A, Miranda V. Spatial-temporal solar power forecasting for smart grids. In: IEEE transactions on industrial informatics,, vol. 1; 2015. p. 232–41.
[34] Antonanzas J, Pozo-Vázquez D, Fernandez-Jimenez LA, Martinez-de-Pison FJ. The value of day-ahead forecasting for photovoltaics in the Spanish electricity market. In: Solar energy, vol. 158; 2017. p. 140–6.
[35] Gutierrez-Corea FV, Manso-Callejo MA, Moreno-Regidor MP, Manrique-Sancho MT. Forecasting short-term solar irradiance based on artificial neural networks and data from neighboring meteorological stations. In: Solar energy, vol. 134; 2016. p. 119–31.
[36] Tascikaraoglu A, Sanandaji BM, Chicco G, Cocina V, Spertino F, Erdinc O, Paterakis NG, Catalão JPS. Compressive spatio-temporal forecasting of meteorological quantities and photovoltaic power. In: IEEE transactions on sustainable energy, vol. 3; 2016. p. 1295–305.
[37] Agoua XG, Girard R, Kariniotakis G. Short-term spatio-temporal forecasting of photovoltaic power production. In: IEEE transactions on sustainable energy, vol. 9; 2018. p. 538–46.
[38] Zhao X, Wei H, Wang H, Zhu T, Zhang K. 3D-CNN-based feature extraction of ground-based cloud images for direct normal irradiance prediction. In: Solar energy, vol. 181; 2019. p. 510–8.
[39] Rodríguez F, Fleetwood A, Galarza A, Fontán L. Predicting solar energy generation through artificial neural networks using weather forecasts for microgrid control". In: Renewable energy, vol. 126; 2018. p. 855–64.
[40] Qing X, Niu Y. Hourly day-ahead solar irradiance prediction using weather forecasts by LSTM. In: Energy, vol. 148; 2018. p. 461–8.
[41] Wang K, Qi X, Liu H. Photovoltaic power forecasting based LSTM-Convolutional Network. In: Energy, vol. 189; 2019. p. 116–225.
[42] Shakya A, Michael S, Saunders C, Armstrong D, Pandey P, Chalise S, Tonkoski R. Solar irradiance forecasting in remote microgrids using markov switching model. In: IEEE transaction on sustainable energy, vol. 8; 2017. p. 895–905.
[43] Paulescu M, Paulescu E. Short-term forecasting of solar irradiance. In: Renewable energy, vol. 143; 2019. p. 985–94.
[44] Sain-Drenan YM, Bofinger S, Fritz R, Vogt S, Good GH, Dobschiski J. An empirical approach to parameterizing photovoltaic plants for power forecasting and simulation. In: Solar energy, vol. 120; 2015. p. 479–93.
[45] Jiang H, Dong Y. Global horizontal radiation forecast using forward regression on a quadratic kernel support vector machine: case study of the Tibet Autonomous Region in China. In: Energy, vol. 133; 2017. p. 270–83.
[46] Chen SX, Gooi HB, Wang MQ. Solar irradiation forecast based on fuzzy logic and neural networks. In: Renewable energy, vol. 52; 2013. p. 118–27.
[47] Orfila A, Ballester JL, Oliver R, Alvarez A, Tintoré J. Forecasting the solar cycle with genetic algorithms. In: Astronomy & astrophysics, vol. 386; 2002. p. 313–8.

[48] Shaddel M, Seyed D, Baghernia P. Estimation of hourly global solar irradiation on tilted absorbers from horizontal one using Artificial Neural Network for a case study of Mashhad. In: Renewable and sustainable energy reviews, vol. 53; 2016. p. 59–67.
[49] Goodfellow I, Bengio Y, Courville A. Deep learning. MIT Press; 2016.
[50] Ortiz-García EG, Salcedo-Sanz S, Casanova-Mateo C, Paniagua-Tineo A, Portillas-Figueras JA. Accurate local very-short term temperature prediction based on synoptic situation Support Vector Regression banks. In: Atmospheric research, vol. 107; 2012. p. 1–8.
[51] Sivaneasan B, Yu CY, Goh KP. Solar forecasting using ANN with fuzzy logic preprocessing. In: Energy procedia, vol. 143; 2017. p. 727–37.
[52] Chu Y, Coimbra CFM. Short-term probabilistic forecast for direct normal irradiance. In: Renewable energy, vol. 101; 2017. p. 526–36.
[53] Yang X, Abbes D, Francois B. Uncertainty analysis for day ahead power reserve quantification in an urban microgrid including PV generators. In: Renewable energy, vol. 106; 2017. p. 288–97.